Heliyon 9 (2023) e14394

Contents lists available at ScienceDirect

Heliyon

journal homepage: www.cell.com/heliyon

Research article

Detecting abnormal seismic activity areas of Anatolian plate and deformation directions using Python Geospatial libraries

Hakan Güneyli [a], Shaheen Mohammed Saleh Ahmed [b,*]

[a] Department of Geology, Cukurova University, Balcali-Adana, Turkey
[b] Department of Geology, College of Science, Kirkuk University, Kirkuk, Iraq

ARTICLE INFO

Keywords:
Deformation
Anatolian plate
Seismogenic
Geostatistical analysis
Arabian

ABSTRACT

Various inaccurate traditional models have resulted in major ambiguities and gaps in the interpretation of Anatolian plate deformation directions. To address this issue, a GIS-based spatial statistical analysis method was used for the first time to detect the directional distribution of deformation along the Anatolian Plate in Turkey. Two strategies were used in this study: firstly, identifying the abnormally active seismic areas by detecting significant hotspot and cold spot clusters and confirming this detection using optimized hotspot analysis for earthquake events that occurred from 1900 to the end of 2019. Secondly, detecting the directional distribution of deformation using a Standard Deviational Ellipse (SDE) by calculating the standard deviation of the x and y coordinates from the mean center for each set of earthquake events in the Anaconda Python Platform and ArcGIS 10.8 software. Our improved geostatistical analysis results confirmed the existence of abnormal seismic hazard zones within the study area and three deformation directions: the east-west trend, the southeast-northwest trend, and the south-north trend.

1. Introduction

The activity of the Anatolian plate is influenced by the collision of the African, Arabian, and Anatolian plates, resulting in the westward displacement of Anatolia along the North Anatolian Fault (NAF) and East Anatolian Fault (EAF) intra-continental fault zones [1–14]. This deformation is observed throughout the study area, with three distinct deformation stages proposed by Ref. [15]: Middle Eocene-Middle Miocene NW-SE extension deformation, Late Miocene-Early Pliocene NNE-SSW compression deformation, and Late Pliocene strike-slip tectonic deformation [16,17]. used direct inversion (INVD) based on Wallace-Bott's analysis of more than 200 fault slips measured in 80 different positions in the north Anatolian plate principal [18,19] to confirm these findings. The westward motion of the Anatolian plate as shown in Figure (1) is a major cause of the deformation, which is believed to be driven by the southward forces of the Aegean rather than the pushing forces of the Arabian plate on the Anatolian plate's edge. As per [20], the Anatolian plate was once a single plate that is currently breaking up into multiple smaller plates, with the earliest stage of separation occurring in southeastern Anatolia during the Paleocene and Middle Eocene.

In order to investigate the deformation directions of the Anatolian Plate, this study employed spatial statistical analysis of earthquakes that occurred between 1900 and the end of 2019, ensuring that these earthquakes were not randomly distributed. The study employed two strategies: the first identified abnormally active seismic areas through the identification of significant hotspot and cold spot clusters and confirmed these findings through optimized hotspot analysis of earthquakes between 1900 and the end of 2019.

* Corresponding author.
E-mail address: shaheengeolo@gmail.com (S.M. Saleh Ahmed).

https://doi.org/10.1016/j.heliyon.2023.e14394
Received 6 April 2022; Received in revised form 25 February 2023; Accepted 2 March 2023
Available online 8 March 2023
2405-8440/© 2023 The Authors. Published by Elsevier Ltd. This is an open access article under the CC BY-NC-ND license (http://creativecommons.org/licenses/by-nc-nd/4.0/).

The second strategy utilized the Standard Deviational Ellipse (SDE) to detect the directional distribution of deformation, with the aim of determining the spatial deformation features and directional tendency of the Anatolian Plate.

2. Data

2.1. Remote sensing data

This paper utilizes the ETOPO1 model, which is a high-resolution global relief model of the Earth's surface at a 1 arc-minute resolution that integrates both land topography and ocean bathymetry. The model is considered an excellent base map for this study since it accurately reflects the actual volumes of the world's oceans and the true hypsographic curves (cumulative elevations) of the Earth's surface. The ETOPO1 model was constructed using data sets from the National Geophysical Data Center (NGDC), a division of the National Oceanic and Atmospheric Administration (NOAA) on a global scale [21]. Downloaded from https://www.ngdc.noaa.gov/mgg/global.

2.2. Geographic information data

The Earthquake Hazard Program of the USGS provided a GIS shape file of a catalog containing historical earthquakes in the Middle East region and total earthquakes from 1900 to 2019 for the Anatolian Plate and neighboring countries (Table 1). This catalog covers earthquake sources that can pose a significant hazard for the Anatolian Plate and includes recorded earthquakes with magnitudes ranging from 4 to 8 on the unified Mw magnitude scale. Aftershocks, foreshocks, and swarm-type activities were excluded from the catalog to ensure its homogeneity. The density of earthquakes was estimated by fitting a smoothly tapered surface to the location of each earthquake using the magnitude as a weight and a kernel function in the GIS.

Additionally, the General Directorate of Mineral Research and Exploration's Series of Extraordinary Publications—30 provided a Turkey Active Fault Map at a scale of 1:50,000.

3. Methodology

3.1. Spatial statistical analysis

Spatial statistics refer to the use of statistical methods to analyze and describe the distribution of events in space, with a specific

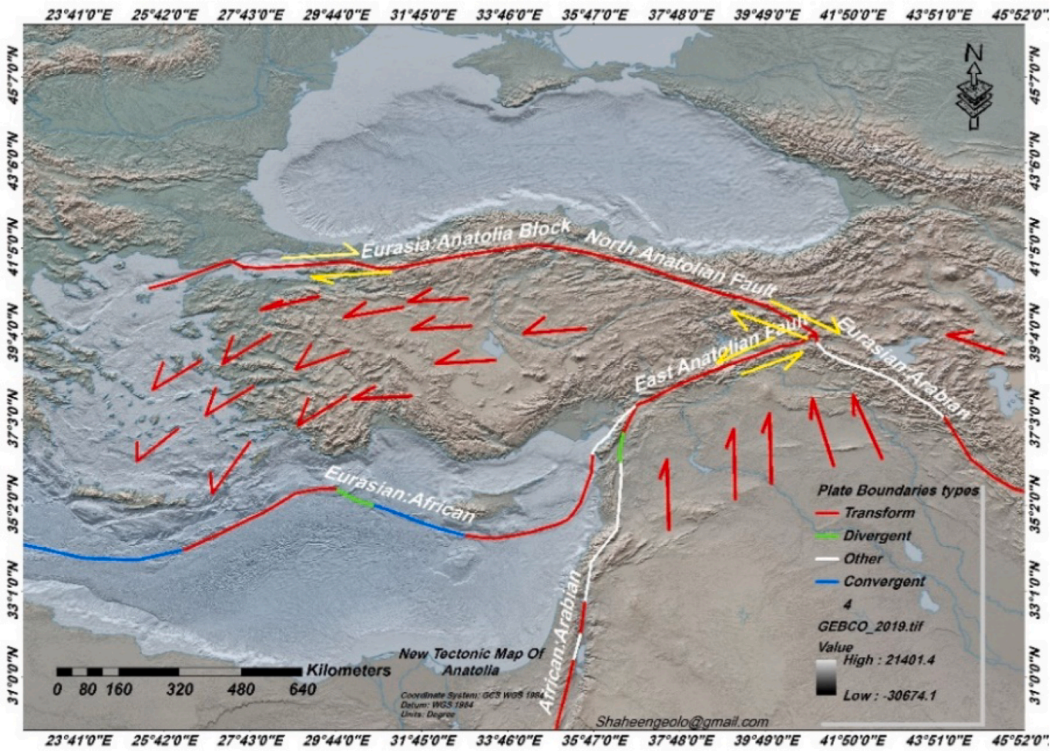


Fig. 1. The Anatolian plate's westward motion, which was one of the main reasons for Anatolian deformation.

Table 1
The compiled catalog includes the recoded earthquakes in the range of 4 ≤ m ≤ 8 of different magnitude scales covering the time interval from 1900 to 2009.

time	latitude	longitude	depth	mag	Mag type	nst	gap	dmin
2023-02-03T01	37.1997	36.5107	10	4.2	mb	33	137	0.559
2023-01-31T04	38.5432	44.878	10	4	mb	26	82	1.447
2023-01-29T09	38.5646	44.784	10	4.2	mb	34	143	1.378
2023-01-29T10	38.573	44.5857	10	4.1	mb	17	179	1.227
2023-01-29T13	35.7754	35.7382	10	4.3	mb	27	132	1.83
2023-01-29T15	38.41	44.8049	10	4.5	mb	35	152	1.376
2023-01-29T14	38.5096	44.7975	10	4.7	mb	32	146	1.38
2023-01-29T03	38.6464	44.8532	10	4.1	mb	17	127	1.502
2023-01-28T20	38.5084	44.8234	10	4.5	mb	29	83	1.4

emphasis on spatial data [22]. In the present time, there have been significant advancements in both technical and theoretical aspects of GIS science, which have greatly benefited spatial statistics. Nonetheless, with the increased usage of spatial statistics in diverse fields, it has become essential to enhance the interaction between methodologies, computational capabilities, and the distinct characteristics of each discipline. Our approach is uncomplicated, and we have followed the procedures outlined in Fig. 2.

3.1.1. Geospatial clustering

Geospatial clustering is the process of categorizing a set of spatial objects into groups or "clusters" based on their similarities. The objective of clustering is to identify relationships between spatial and non-spatial attributes and generate generalizations. Before conducting hotspot analysis, it is crucial to examine the data for clustering through preliminary analysis techniques such as spatial autocorrelation. This technique detects the presence of clustering in the original dataset, with two methods available: Moran's I (global) and Getis-Ord General G (global). The output of these methods includes a z-score that, when combined, indicates whether or not clustering exists in the data.

3.1.1.1. Local and global spatial statistical analyzes procedures. The objective of local statistics is to examine and discover spatial relationships, variations between variables, and the presence of hot and cold spots or clusters within a given area [23]. In this study, two specific local statistical techniques were employed: (A) Anselin local Moran's I and (B) Getis–Ord Gi*. These methods were utilized to identify any clusters that may exist within the data (hot and cold spots). Getis–Ord Gi*, which were applied to look for clusters if they existed (hot and cold spots).

3.1.1.1.1. Moran's local Anselin I. In order to detect and identify local clusters and spatial outliers [24], suggested the use of a local Moran's I index of spatial autocorrelation, which can be estimated using the following formula:

$$I = \frac{\sum_{1}\sum_{ij} w_y (x_i - \bar{x})(x_j - \bar{x})}{s^2 \sum_{i}\sum_{j} w_i j}$$

where xi, which represents the attribute of feature i, X, which represents the mean attribute value, and Wi,j, which represents the weight of the spatial relationship between features i and j.

Positive values of the Anselin local Moran's I index suggest the existence of neighboring events with similar high or low values, which implies the presence of a local cluster.

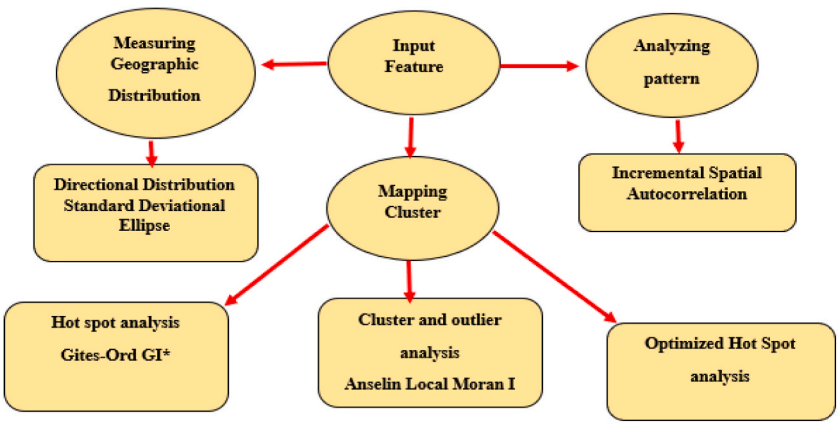


Fig. 2. Sschematic Diagram of this paper methodology procedures.

*3.1.1.1.2. Getis–Ord *.* The statistical significance of identifying hot and cold spots within events can be determined by using the Getis-Ord G* statistic, which is estimated using the following formula:

$$G_i*(d)=\frac{\Sigma_j w_{ij}(\mathrm{d})x_j-\bar{x}\Sigma_j w_{ij}(\mathrm{d})}{s\frac{\sqrt{n\Sigma_j w_{ij}^2-\left(\Sigma_j w_{ij}|d|\cdot\right)}}{n-1}}$$

The attribute value of feature j denoted as xj and the spatial weight between features i and j denoted as win [23].

3.1.2. Hotspot analysis

Hotspot analysis is a mapping and spatial analysis method that focuses on identifying clusters of spatial phenomena. These phenomena are represented as points on a map and correspond to the locations of objects or events. A hotspot can be defined as an area with a higher density of events than would be expected under a random distribution of events. This technique has developed from the examination of point distributions or the way in which points are arranged within a space [25]. In the analysis of point patterns, the concentration of points within a specific region is evaluated against a model of complete spatial randomness, which represents a scenario where point events occur purely at random. In addition to density assessment, hotspot methods are employed to quantify the level of point-event interaction and gain insight into spatial patterns [26]. In the last few decades, the use of hotspot analysis in seismic data analysis has surged, primarily attributed to the emergence of software based on geographic information systems (GIS).

Hotspot analysis employs vector techniques to identify statistically significant hot and cold spots within data by consolidating occurrence points into polygons or merging closely-spaced points based on a calculated distance. When data displays clustering of similar high (hot) or low (cold) values, analysis groups are established.

3.1.3. Optimized hot spot analysis (OHS)

The Hot Spot Analysis (Getis-Ord Gi*) tool utilized in OHS Analysis utilizes variables derived from input data to conduct its analysis. Similar to a digital camera's fully automatic setting that utilizes illumination and subject to ground readings to determine the optimal aperture, shutter speed, and focus, the OHS Analysis tool examines the data to identify the ideal settings for producing optimal hot spot results. If the input data includes incident point data, the tool will aggregate the incidents in weighted features (as illustrated in Fig. 3) and determine the appropriate measure of analysis based on the distribution of the measurement strategy. The statistical significance observed in the Output Features will be automatically corrected for multiple testing and spatial dependence using the False Discovery Rate (FDR) correction method [22,23].

3.1.4. Standard deviational ellipse (SDE])

The SDE summarizes the structural rigidity and directional trend (bias) of the geographic distribution by measuring the diffusion (spread) of the data. This measure calculates the standard distance separately in the x and y directions (as shown in Fig. 4 and Equations (1) and (2)) [28].

$$SD_x=\sqrt{\sum_{i=1}^{n}(X_i-\overline{X})^2\Big/n} \tag{1}$$

$$SD_y=\sqrt{\sum_{i=1}^{n}(Y_i-\overline{Y})^2\Big/n} \tag{2}$$

"n" represents the total count of spatial objects, such as points or polygons. The coordinates of the i-th spatial object are given by xi and yi, while $\overline{X}$ and $\overline{Y}$ refer to the coordinates of the mean center [28].

The SDE is characterized by two standard distances that are perpendicular to each other, with the ellipse being centered on the mean center and rotated at an angle θ measured from north to south.

If $x_i^{'}=x_i-\overline{X}$ and $Y_i^{'}=Y_i-\overline{Y}$ are the deviations of the points form the mean center, the rotation angle is calculated by equation (3)

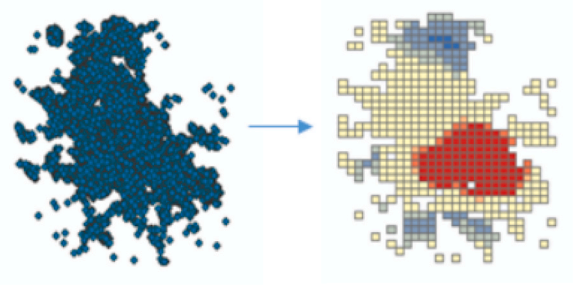


Fig. 3. Illustration of Optimized Hot Spot Analysis from ArcGIS Pro 2.8 Help [27] archive.

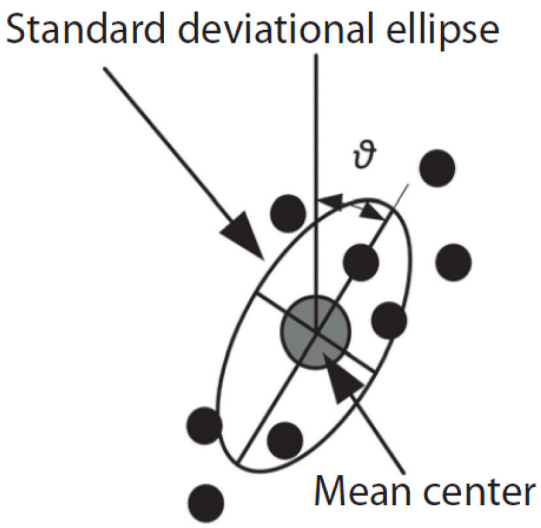


Fig. 4. Standard deviational ellipse explanation diagram of dispersion and directional trend in GIS. The figure from the official [ESRI] ARCGIS help [29].

[23]:

$$\tan\theta = \frac{\left(\sum_i^n x_i'^2 - \sum_i^n y_i'^2\right) + \sqrt{\left(\sum_i^n x_i'^2 - \sum_i^n y_i'^2\right)^2 + 4\left(\sum_i^n x' \sum_i^n y'\right)^2}}{2\sum_i^n x_i' \sum_i^n y_i'} \tag{3}$$

The rotation angle θ corresponds to the angle between the major axis and north. A positive tangent signifies a clockwise rotation of the major axis from north to south, while a negative tangent indicates a counterclockwise rotation of the ellipse from north to south.

The orientation and size of the ellipse can also be determined based on the weighted locations of an attribute. The direction of the ellipse reveals any directional biases that may be further investigated in relation to the problem at hand. Comparing the size and orientation of two or more ellipses can also reveal different spatial patterns. A standard deviational ellipse typically encloses approximately 63% of the features when the underlying spatial pattern is focused on a core with fewer objects dispersed around it. This rule of thumb is based on the Rayleigh distribution. For two-dimensional data, two standard deviations would encompass approximately 98% of the events, while three standard deviations would cover almost all the features (99.9%). For a non-spatial one-dimensional variable, the corresponding percentages for the normal distribution and standard deviation statistics are 68%, 95%, and 99%. Calculating a standard deviational ellipse yields an ellipse centered on the mean center of all objects, two standard distances (representing the length of the long and short axes), and the orientation of the ellipse. The axis rotation is determined such that the sum of the squares of the distances between the points and the axes is minimized. The standard deviational ellipse is a more descriptive measure than the standard distance and is more commonly used.

4. Results and discussions

To extract the abnormally active seismic areas and the directions of deformation along the Anatolian Plate, Turkey, this paper used two strategies.

4.1. First strategy identifying abnormal active seismic areas

Initially, spatial autocorrelation using Moran's I was employed to distinguish between random and spatially related patterns. Our dataset underwent a test for complete spatial randomness, which resulted in rejecting the null hypothesis, indicating the presence of spatial relationships. The spatial autocorrelation report (Fig. 5) revealed a score of 22.610 and a p-value of 0.0001, indicating a less than 1% chance that the clustered pattern in the data arose due to random chance.

4.1.1. Identification of significant hotspots and cold spot clusters

This study utilized both the ArcToolbox spatial statistics toolbox and the Python framework of ARCGIS 10.8 software. Initially, we employed the Cluster and Outlier Analysis [Anselin Local Morans I] tool from the mapping cluster subclass of spatial statistics tools to analyze the feature attribute points of the earthquake catalog. The magnitude of earthquakes was selected as the input feature class to generate an output feature class containing the visualization of hot and cold spots. To define the neighborhoods around each feature, we had to conceptualize a spatial relationship and specify the neighbors' distance using the INVERSE_DISTANCE option. The resulting

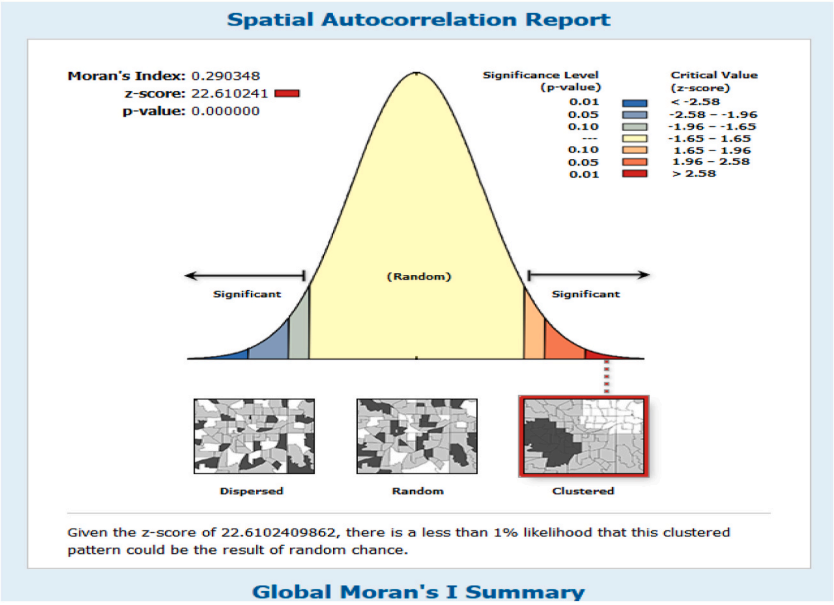


Fig. 5. Spatial Autocorrelation Report (Global Moran's I summary) Global Moran's I summary.

output, shown in Fig. 6, displays the Gi_Bin field, which categorizes the dataset into ranges of three for both cold and hot spots with 90%, 95%, and 99% confidence levels. The results revealed a high density of 99% confidence red hot spots with static signatures along the North Anatolian plate fault zone, the Eastern Anatolian plate fault zone, and the Southwest Anatolian plate zone. Additionally, blue cold spots with high significance were observed in the far west and north of the Anatolian plate fault system, with a low density near the Aegean Sea. The Cluster and Outlier Analysis tool enables us to differentiate between random and spatially dependent patterns, and in this study, the null hypothesis of complete spatial random chance was rejected based on the spatial autocorrelation report (Fig. 5), indicating that our data has a clustered pattern that is not due to random chance.

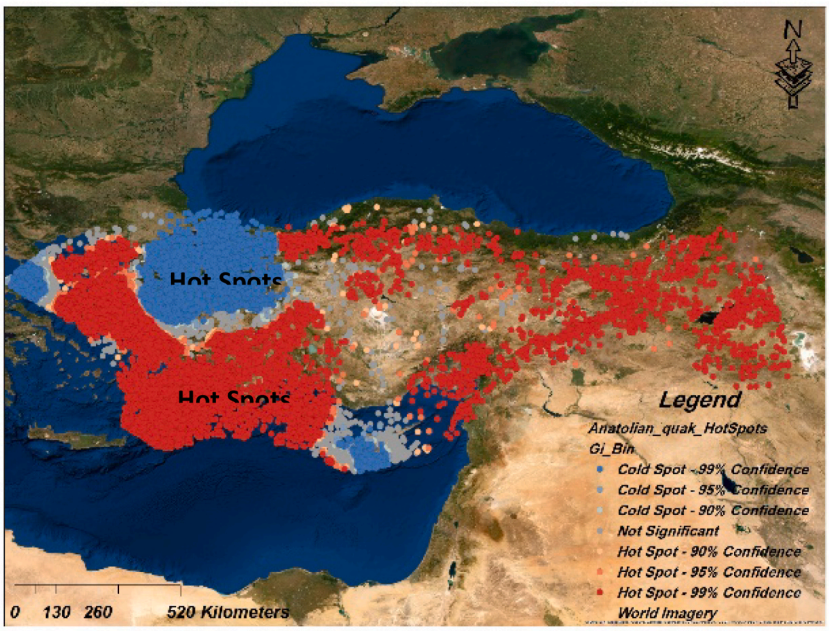


Fig. 6. The Cluster and Outlier Analysis [Anselin Local Morans I] tool results show the hot spot [Red points] and cold spot [blue points] maps of Anatolian and the Gi_Bin field classifications.

Table 2
Z_score and P_value results showing obvious spatial clustering for this research earthquake dataset.

Moran Index	0.29
Z_score	22.61
P_values	0.0001

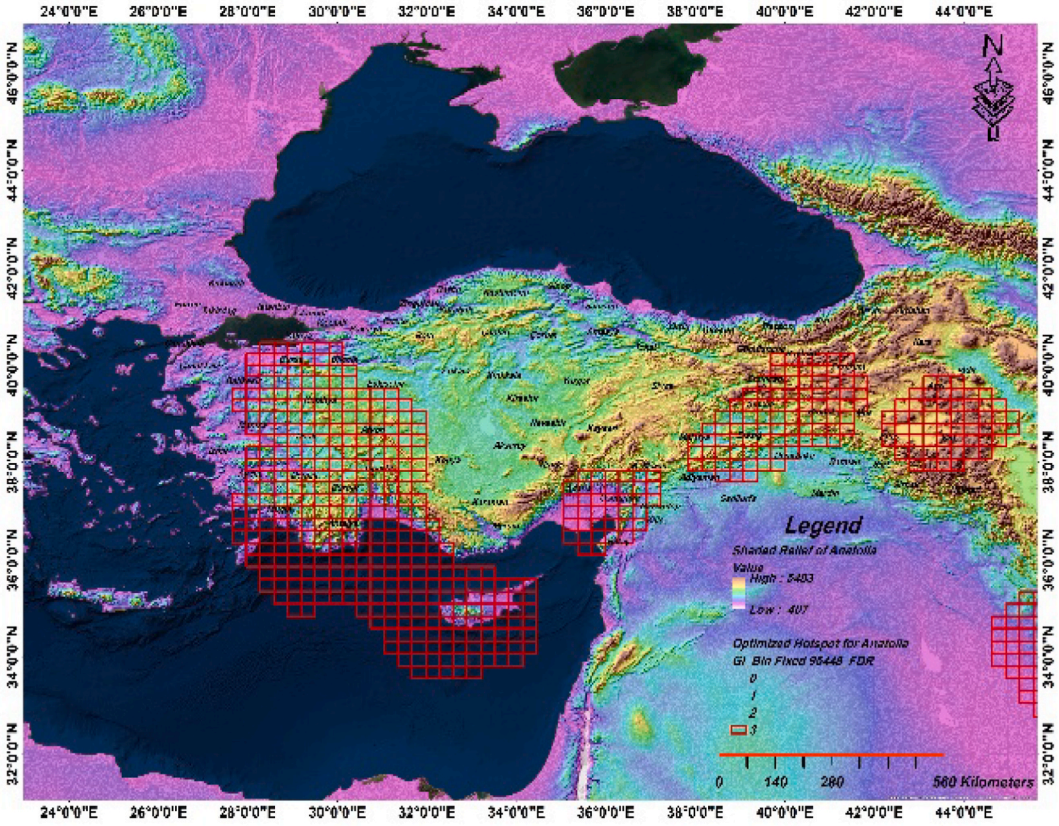


Fig. 7. The high +3 Gi_Bin value resulted from Optimized Hot spot map for Anatolian, which is indicated by fixed red rectangular regions

4.1.2. Optimized hot spot analysis of Anatolian plate

The study employed the optimized hot spot (OHS) analysis to identify clusters that contribute to statistical hot spots. To conduct the analysis, we utilized the optimized hot spot analysis tool from the mapping cluster subclass of spatial statistics tools, which enables rapid hotspot analysis. The earthquake catalog points were designated as the input dataset, and we selected the incident data clustering method [COUNT_INCIDENTS_WITHIN_AGGREGATION_POLYGONS] and the Polygons Grouping Occurrences Into Count Data option for nearby features within the tool. The tool aggregated the point data in neighboring polygons to identify hot and cold spots in the data. The significance of the hot and cold spots was determined based on the z-score and p-value, where a feature with a low p-value and a high z-score indicates a significant hotspot, and a low negative z-score and small p-value suggests an important cold spot. A z-score close to 0 indicates no spatial clustering. According to Table 2, the z-score is 22.610, and the p-value is low at 0.00001, indicating a clear spatial clustering in the study dataset. The optimized hot spot map of the Anatolian Plate is shown in Fig. 7, where the Gi_Bin field identifies statistically significant hot and cold spots, and the +3 bins represent statistical significance with a 99% confidence level.

4.2. The result of the first strategy

Local statistics were employed to investigate the occurrence and distribution of seismic clusters or "hot spots" on the Anatolian Plate between 1900 and 2019. Moran's I and Getis-Ord Gi were utilized to generate Fig. 8, which displays the hot spot and cold spot patterns of seismic events based on their magnitudes. Red dots indicate high-magnitude earthquakes [$>$ 4.5 MW] that are surrounded by similar strong seismic events, while blue dots represent low-magnitude earthquakes that are surrounded by other weak seismic events $\leq$ 4.5 MW.

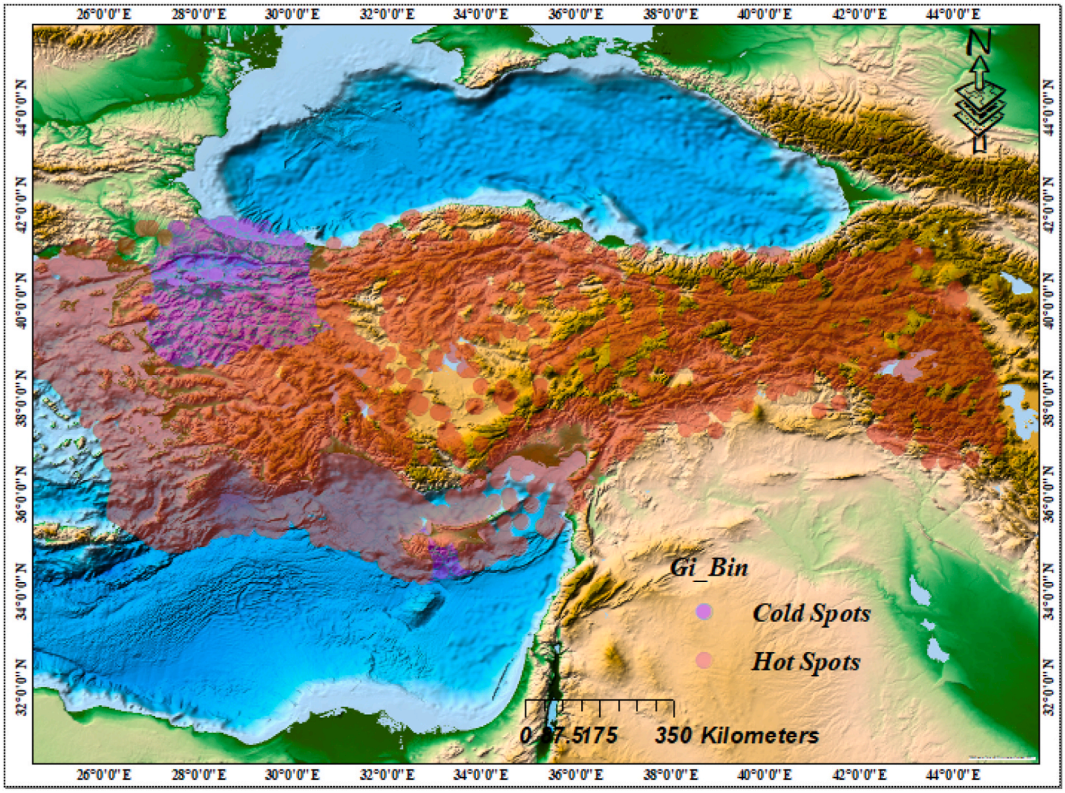


Fig. 8. Abnormal seismic activity regions of the Anatolian Plate represented by the red points that are hot spots indicate earthquakes of large magnitude >4.5 mw and the blue points that are cold spots indicate low-magnitude seismic events ≤ 4.5 mw.

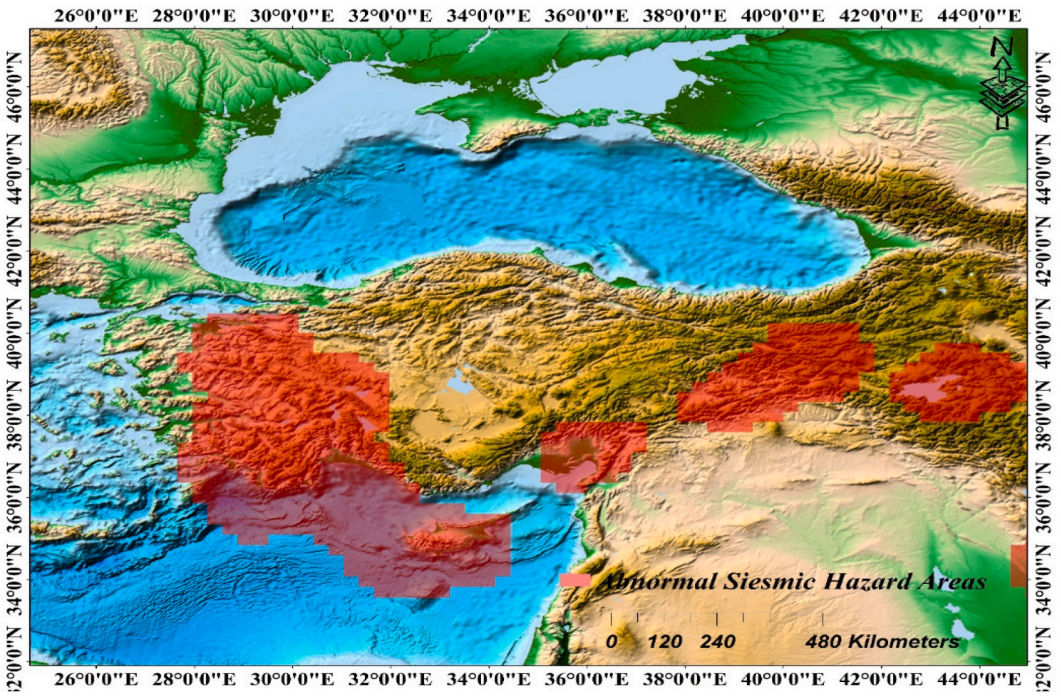
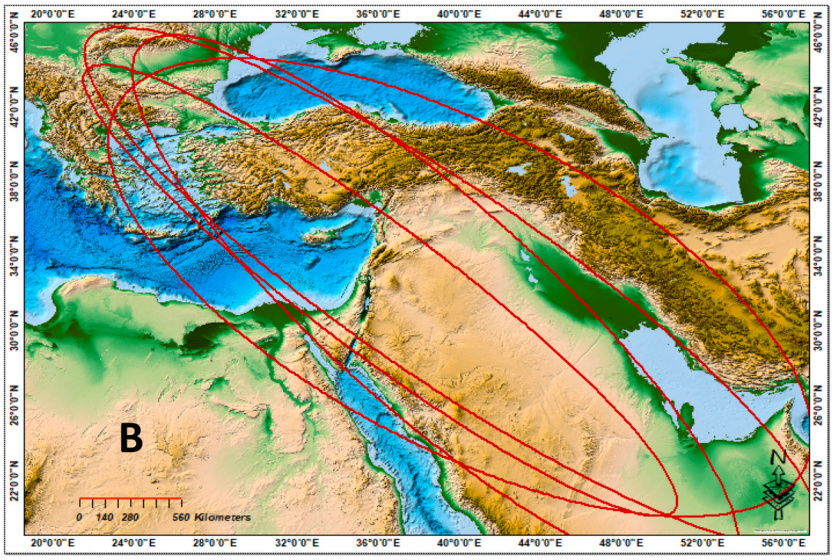
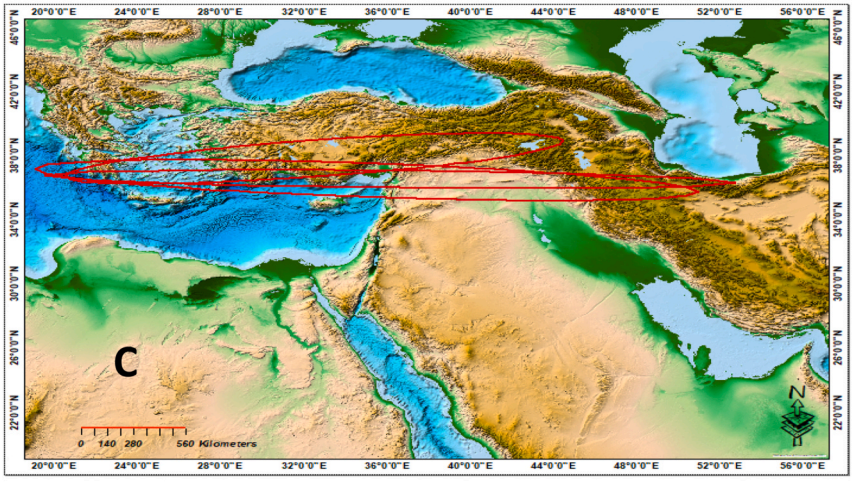
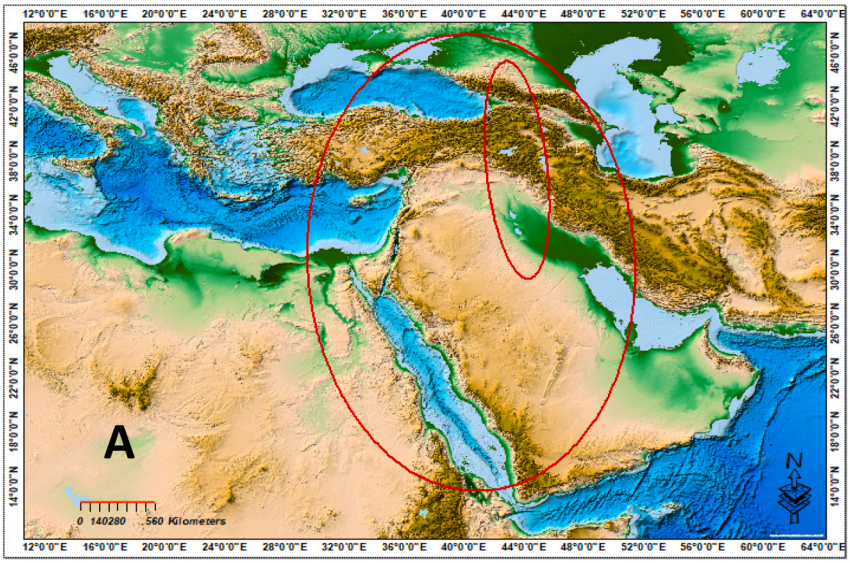


Fig. 9. The most active abnormal seismic regions constructed using OHS results and Turkey's Active Fault Map, which illustrates abnormal seismic hazard along the East Anatolian Fault Zone EAFZ] and West Anatolian Fault System [WAFS].







(caption on next page)

Fig. 10. The directions of deformation along the Anatolian plate. A] Deformation from south to North B] Deformation from Southeast to northwest. C] Deformation from east to west.

The visualization in Fig. 9 shows the most active abnormal seismic regions constructed using OHS results and depicts elevated concentrations of clusters in various regions of Turkey, including the eastern, western, southeastern, and northern parts. Conversely, in the western area of the Anatolian Plateau, there are noteworthy low-density regions. Despite their theoretical underpinnings, statistical foundations, or mathematical interpretations, all spatial clustering approaches have shortcomings concerning precision, responsiveness, and computational requirements for identifying clusters, as indicated by our OHS findings.

4.3. Directional distribution of deformation [second strategy]

After analyzing the hot and cold spots, we utilized the improved directional distribution analysis (ISDE) to investigate the spatial distribution of these areas and explore the directional tendency and spatial deformation characteristics of the Anatolian Plate. Our method comprises two types of directional deformation distribution techniques. The first technique involves calculating the standard deviation of the x and y coordinates from the mean center for each hot and cold spot region, and an ellipse is derived from the calculations to determine if earthquakes are distributed in an elongated pattern. The second technique is similar to the first, but instead of a set of earthquake events, it measures and calculates for every individual earthquake. Our findings reveal three directions of deformation affecting the Anatolian Plate, namely from south to north, southeast to northwest, and east to west, which are presented in Fig. [10 A, B, and C].

4.4. Geological interpretation of these deformations

The primary factors responsible for these deformations are the collision between the Arabian and Anatolian plates, resulting in crustal thickening in eastern Turkey and compressional deformation along the Bitlis suture zone [30–32]. Furthermore, the North Anatolian Fault Zone (NAFZ) is a complex regional-scale deformation zone and the most significant structural component of the North Anatolian Plate's shear zone [33]. The westward extrusion of the Anatolian Plate Block relative to Eurasia causes intense kinematic deformation within the block's interior. Weak zones within the NAFZ and EAFZ facilitated the movement of the entire Anatolian Plate.

Our findings align well with regional tectonics. Moreover, the Anatolian Plate's deformation has created a lithosphere rich in faults, which are surface manifestations of internal deformation [34]. Deformations have resulted in the expansion of pre-existing faults and the formation of new horizontally and vertically extended faults, indicating that the Anatolian Plate has fragmented into numerous small tectonic plates. This confirms the discovery by Ref. [20] that the region of East Anatolia has nine nanoplates, West Anatolia has six nanoplates, and the core Anatolian Plate region has one nanoplate, following the formation of the Anatolian Plate.

5. Conclusion

The Anatolian Plate's interior exhibits significant kinematic deformation types that have occurred from the Cretaceous to the present day. These deformations have resulted in the expansion of pre-existing faults and the formation of new horizontally and vertically extended faults, creating a lithosphere rich in faults. Based on our analysis, we draw the following conclusions.

- This study is the first to use GIS to enhance spatial statistical methods for analyzing the directional distribution of plate tectonic deformations.
- Our research identified three major deformation directions within the Anatolian Plate: east-west, southeast-northwest, and south-north trends. These deformation directions suggest that the fault network is more widespread throughout the Anatolian Plate, particularly in the east and southeast, than in the western Anatolian zone.
- Earthquakes within the study area occur at a seismogenic depth of approximately 5–10 km, indicating that deformations primarily occur in the upper crust of the Anatolian Plate.

Further research is necessary to understand the causes of these deformations, and we recommend updating the seismic hazard zones map for the study region.

Author contribution statement

Shaheen Mohammed Saleh Ahmed: Conceived and designed the experiments; Performed the experiments; Analyzed and interpreted the data; Wrote the paper. Hakan Güneyli: Analyzed and interpreted the data; Contributed reagents, materials, analysis tools or data.

Funding statement

This research did not receive any specific grant from funding agencies in the public, commercial, or not-for-profit sectors.

Data availability statement

The authors do not have permission to share data.

Declaration of interest's statement

The authors declare the following conflict of interests: Detecting Abnormal Seismic Activity Areas of Anatolian and deformation directions using Python Geospatial libraries The authors whose names are listed immediately below certify that they have NO affiliations with or involvement in any organization or entity with any financial interest [such as honoraria; educational grants; participation in speakers' bureaus; membership, employment, consultancies, stock ownership, or other equity interest; and expert testimony or patent-licensing arrangements], or non-financial interest [such as personal or professional relationships, affiliations, knowledge or beliefs] in the subject matter or materials discussed in this manuscript. Author's name Author's signature Date SHAHEEN AHMED SHAHEEN 2022/04/06 HAKAN GUNEYLE HAKAN 2022/04/06.

References

[1] A. Fichtner, J. Trampert, P. Cupillard, E. Saygın, T. Taymaz, Y. Capdeville, A. Villaseñor, Multiscale full waveform inversion, Geophys. J. Int. 194 (2013) 534–556.
[2] A. Fichtner, E. Saygın, T. Taymaz, P. Cupillard, Y. Capdeville, J. Trampert, The deep structure of the North Anatolian plate fault zone, Earth Planet Sci. Lett. 373 (2013) 109–117.
[3] E.J. Fielding, P.R. Lundgren, T. Taymaz, S. Yolsal-Cevikbilen, S.E. Owen, Fault-slip source models for the 2011M7.1 van earthquake in Turkey fromSAR interferometry, pixel offset tracking, GPS and seismic waveform analysis, Seismol Res. Lett. 84 (2013) 579–593.
[4] D. McKenzie, Active tectonics of Mediterranean region, Geophys. J. Roy. Astron. Soc. 30 (1972) 109–185.
[5] T. Taymaz, J. Jackson, R. Westaway, Earthquakemechanisms in the hellenic trench near crete, Geophys. J. Int. 102 (1990) 695–731.
[6] T. Taymaz, J.A. Jackson, D. Mckenzie, Active tectonics of the North and central aegean sea, Geophys. J. Int. 106 (1991) 433–490.
[7] T. Taymaz, R. Westaway, R. Reilinger, Active faulting and crustal deformation in the Eastern Mediterranean region, Tectonophysics 391 (1–4) (2004) 375.
[8] T. Taymaz, J. Wright, S. Yolsal, O. Tan, E. Fielding, G. Seyitoğlu, Source characteristics of the 6 June 2000 Orta–Çankırı [Central Turkey] earthquake: a synthesis of seismological, geological and geodetic [InSAR] observations, and internal deformation of the Anatolian plate Plate, the geodynamics of the Aegean and Anatolia, Geol. Soc. Lond. Spec. Publ. 291 (2007) 259–290.
[9] T. Taymaz, Y. Yilmaz, Y. Dilek, The geodynamics of the Aegean and Anatolia: introduction, Geol. Soc. Lond. Spec. Publ. 291 (2007) 1–16.
[10] E.A. Vanacore, T. Taymaz, E. Saygın, Moho structure of the Anatolian plate plate from receiver function analysis, Geophys. J. Int. 193 (1) (2013) 329–337.
[11] S. Yolsal-Çevikbilen, Seismic anisotropy along the Cyprean arc and northeast Mediterranean Sea inferred from shear wave splitting analysis, PEPI 233 (2014) 112–134.
[12] S. Yolsal-Çevikbilen, C.B. Biryol, S. Beck, G. Zandt, T. Taymaz, H.E. Adıyaman, A. Özacar, 3D crustal structure along the North Anatolian plate Fault Zone in north-central Anatolia revealed by local earthquake tomography, Geophys. J. Int. 188 (2012) 819–849.
[13] S. Yolsal-Çevikbilen, T. Taymaz, Earthquake source parameters along the Hellenic subduction zone and numerical simulations of historical tsunamis in the Eastern Mediterranean, Tectonophysics 536–537 (2012) 61–100.
[14] H. Gürsoy, J.D.A. Piper, O. Tatar, Neotectonic deformation in the western sector of tectonic escape in Anatolia: palaeomagnetic study of the Afyon region, central Turkey, Tectonophysics 374 (2003) 57–79.
[15] M. Köküm, M. İnceöz, Structural analysis of the northern part of the East Anatolian plate Fault System, J. Struct. Geol. (2018), https://doi.org/10.1016/j.jsg.2018.06.016.
[16] J. Angelier, Tectonic analysis of fault-slip data sets, J. Geophys. Res. 89 (1984) 5835–5848.
[17] J. Angelier, Inversion of field data in fault tectonics to obtain regional stress. III. A new rapid direct inversion method by analytical means, Geophys. J. Int. 103 (1990) 363–376.
[18] R.E. Wallace, Geometry of shearing stress and relation to faulting, J. Geol. 69 (1951) 118–130.
[19] M.P.H. Bott, The mechanics of oblique-slip faulting, Geol. Mag. 96 (1959) 109–117.
[20] Shaheen Mohammed Saleh Ahmed, Hakan Guneyli [, Improved deep learning [inception] CNN for detecting small tectonic plates of broken Anatolian plate, Turkey, All Earth 33 (1) (2021) 52–65, https://doi.org/10.1080/27669645.2021.1945523.
[21] NOAA National Geophysical Data Center, ETOPO1 1 Arc-Minute Global Relief Model, NOAA National Centers for Environmental Information, 2009. (Accessed 20 August 2019). Accessed.
[22] A. Getis, J.K. Ord, The analysis of spatial association by use of distance statistics, Geogr. Anal. 24 (1992).
[23] J.K. Ord, A. Getis, Local spatial autocorrelation statistics: distributional issues and an application, Geogr. Anal. 27 (1995).
[24] Luc Anselin, Local indicators of spatial association—LISA, Geogr. Anal. 27 (2) (1995) 93–115.
[25] S. Chakravorty, Identifying crime clusters: the spatial principles, Middle States Geographer 28 (1995) 53–58.
[26] A. Baddeley, E. Rubak, J. Møller, Score, pseudo-score and residual diagnostics for spatial point process models, Stat. Sci. 26 (2011) 613–646.
[27] Optimized hot spot analysis [spatial statistics] [ArcGIS Pro 3.1], Retrieved from, https://pro.arcgis.com/en/pro-app, 2020.
[28] Grekousis George, [, Analyzing Geographic Distributions and Point Patterns, Cambridge University Press, 2020. Retrieved from, https://www.cambridge.org.
[29] B. Wang, W. Shi, Z. Miao, Confidence analysis of standard deviational ellipse and its extension into higher dimensional euclidean space, PLoS One 10 (3) (2015), e0118537, https://doi.org/10.1371/journal.pone.0118537.
[30] J.F. Dewey, M.R. Hempton, W.S.F. Kidd, F. Saroglu, A.M.C. Sengor, Shortening of continental lithosphere: the neotectonics of Eastern Anatolian plate—a young collision zone, in: Collision Tectonics, 2022.
[31] M. Keskin, Magma generation by slab steepening and breakoff beneath a subduction-accretion complex: an alternative model for collision-related volcanism in Eastern Anatolian plate, Turkey, Geophys. Res. Lett. 30/24 (2003) 8046.
[32] E. Zor, E. Sandvol, C. Gurbuz, N. Turkelli, D. Seber, M. Barazangi, The crustal structure of the East Anatolian plate plateau [Turkey] from receiver functions, Geophys. Res. Lett. 30/24 (2003) 7.1–7.4.
[33] A. Şengör, O. Tüysüz, C. İmren, M. Sakınç, H. Eyidoğan, N. Görür, X. Le Pichon, C. Rangin, The North Anatolian plate Fault: a new look, Annu. Rev. Earth Planet Sci. 33 (1) (2005) 37–112, https://doi.org/10.1146/annurev.earth.32.101802.120415.
[34] P.C. England, D. Mckenzie, A thin viscous sheet model for continental deformation, Geophys. J. Roy. Astron. Soc. 70 (1982) 295–321.